Discrete-time sliding mode control of a direct-drive robot manipulator

43rd IEEE Conference on Decision and Control
December 14-17, 2004
Atlantis, Paradise Island, Bahamas

Discrete-time Sliding Mode Control of a Direct-drive Robot Manipulator

Geert van der Zalm, Dragan Kostić, *Student Member, IEEE* , and Bram de Jager

Abstract—**This paper investigates the application of a recently introduced discrete-time sliding mode algorithm in robot motion control. The algorithm was developed to ensure chattering-free discrete-time sliding mode control in finite time. Robustness against disturbances and modeling errors are the additional merits of this algorithm. Here, the algorithm is adapted for the robot motion control problem, and it is used to design feedback controllers of a benchmark direct-drive robot. Theory and experiments confirm the applicability of the algorithm. However, they also reveal restrictions in controller tuning, that may result in undesirable amplification of noise and in excitation of parasitic dynamics.**

I. Introduction

THE theory of variable structure systems with sliding mode control (SMC) has been developing for the last five decades [1-8]. Some robotic applications of the theory can be found in [1-4]. Theoretically, when designed in continuous time, SMC features invariance to disturbances and to modeling errors, closed-loop system order reduction, and predictable transient behavior. In practice, especially with discrete-time implementations of SMC algorithms, control chattering occurs due to the finite duration of controller switching. Chattering is an undesirable high-frequency oscillation of the control input that may excite unmodelled dynamics present in electromechanical systems, resulting in decreased control performance.

To deal with problems caused by discrete-time implementation of SMC algorithms, several methodological and conceptual solutions have been proposed. Methodological solutions are directed at eliminating or reducing the effects of chattering [1-4]. The most important conceptual contribution is the development of discrete-time sliding mode control (DSMC) algorithms [5-8] that directly take into account the effects of discretization. The DSMC algorithm considered in [7,8] utilizes both conceptual and methodological advances. It ensures that the sliding mode is reached in finite time without chattering. Additionally, the characteristics of SMC are preserved: the algorithm ensures closed-loop stability in the presence of disturbances and modeling errors [8], enabling nice control over transient behavior of the controlled system. In the absence of disturbances and modeling uncertainties, the order of the closed-loop system is reduced in the sliding mode. A distinguishing property is the simplicity of the DSMC feedback control law, which can be implemented on-line with minimal computational effort.

These merits, seemingly quite appealing, motivated us to investigate the use of the DSMC algorithm in robot motion control, since so far, the algorithm was experimentally tested only for an oscillator design [7] and in the control of a simple linear unloaded DC motor [8]. We present adaptations of the original algorithm [8] that make it applicable for robot motion control. It appears, though, that the obtained chattering-free control law can still cause undesirable amplification of noise and parasitic dynamics, since it features a restriction of the ratio between proportional and derivative feedback gains, inducing high-gain feedback at higher frequencies. The observed problems will be theoretically studied and experimentally demonstrated on a benchmark direct-drive robotic system.

A mathematical formulation of the DSMC algorithm is given in the next section. The robotic set-up used in the experiments is presented in section III. The DSMC design for this robot is demonstrated in section IV. Results of experimental testing are also shown, followed by the conclusions.

II. Mathematical Formulation

A. Robot Dynamics and Model-based Motion Controller

Let us represent the rigid-body dynamics of a serial robotic manipulator with n actuated joints using Euler-Lagrange's equations of motion [9]:

$$\mathbf{M}(\mathbf{q}(t))\ddot{\mathbf{q}}(t)+\mathbf{h}(\mathbf{q}(t),\dot{\mathbf{q}}(t))=\boldsymbol{\tau}(t)+\boldsymbol{\tau}_v(\mathbf{q}(t),\dot{\mathbf{q}}(t),t)\,, \quad (1)$$

where $\boldsymbol{\tau}\in\mathbb{R}^n$ is the vector of joint forces/torques, $\mathbf{M}\in\mathbb{R}^{n\times n}$ is the inertia matrix, $\mathbf{q},\dot{\mathbf{q}},\ddot{\mathbf{q}}\in\mathbb{R}^n$ are the joint motions, speeds, and accelerations, respectively, $\mathbf{h}\in\mathbb{R}^n$ represents Coriolis/centripetal, gravity, and friction effects, $\boldsymbol{\tau}_v\in\mathbb{R}^n$ is the collection of all perturbations in the robot dynamics (e.g. variable friction) and disturbances (e.g., noise and cogging force), and t is time. Assume that models of sufficient quality of $\mathbf{M}$ and $\mathbf{h}$ are available, $\boldsymbol{\tau}_v$ is unknown, and only $\mathbf{q}$ is measurable.

The objective of the motion control problem is steering the joint motions along the reference trajectory $\mathbf{q}_r(t)$. This problem can be solved using $\mathbf{M}$ and $\mathbf{h}$ as follows:

Manuscript received 02 March, 2004.

Geert van der Zalm, (e-mail: geertvanderzalm@hotmail.com, phone: 0031 40 2143508, fax: 0031 40 214 4385), Dragan Kostic, (e-mail: D.Kostic@tue.nl) and Bram de Jager (e-mail: A.G.de.Jager@wfw.wtb.tue.nl) are with the Dynamics and Control Technology Group, Department of Mechanical Engineering, Eindhoven University of Technology, P.O. Box 513, 5600 MB Eindhoven, The Netherlands.

0-7803-8682-5/04/$20.00 ©2004 IEEE

$$\boldsymbol{\tau}(t) = \mathbf{M}(\mathbf{q}(t))\mathbf{u}(t) + \mathbf{h}(\mathbf{q}(t), \dot{\mathbf{q}}(t)), \quad (2)$$

where $\boldsymbol{\tau}$ is the total control law and $\mathbf{u}$ is the feedback control action. The controller (2) realizes feedback linearization [4] of the robot dynamics, since the nonlinear couplings between the robot joints are compensated.

The feedback action $\mathbf{u}$ stabilizes the robot motion and ensures the desired control performance. When applied, the model-based controller (2) reduces the motion control problem to:

$$\ddot{\mathbf{q}}(t) = \mathbf{u}(t) + \mathbf{v}(t) \quad (3)$$

where

$$\mathbf{v}(t) = -\mathbf{M}^{-1}(\mathbf{q}(t))\boldsymbol{\tau}_v(\mathbf{q}(t), \dot{\mathbf{q}}(t), t) \quad (4)$$

The dynamics (3) that remain after feedback linearization are treated next.

B. Uncompensated Dynamics and Reconstruction of States

The following mathematical formulation assumes the presence of a time-delay in the position measurements, which is constant and an integer multiple of the sampling period. This assumption is necessary for the case-study presented later on in the paper. It is also assumed that the reference trajectory is known, so $\mathbf{u}$ can be postulated as

$$\mathbf{u}(t) = \ddot{\mathbf{q}}_r(t) + \mathbf{u}^*(t) \quad (5)$$

where $\ddot{\mathbf{q}}_r$ is the reference acceleration and $\mathbf{u}^*$ the discrete-time sliding mode controller output. To design such a controller, we define the position error as

$$\mathbf{e} = \mathbf{q} - \mathbf{q}_r \quad (6)$$

Substituting (6) in (3), and taking into account (5), gives

$$\ddot{\mathbf{e}}(t) = \mathbf{u}^*(t) + \mathbf{v}(t) \quad (7)$$

A state-space representation of the ith equation of (7), corresponding to the i-th joint ($i = 1, \ldots, n$), has the form

$$\dot{\mathbf{x}}_i^e(t) = \mathbf{A}_i^e \mathbf{x}_i^e(t) + \mathbf{b}_i^e(u_i^*(t) + \nu_i(t)) \quad (8a)$$

$$\mathbf{x}_i^e(t) = [e_i(t), \dot{e}_i(t)]^T, \ \mathbf{A}_i^e = \begin{bmatrix} 0 & 1 \\ 0 & 0 \end{bmatrix}, \text{ and } \mathbf{b}_i^e = \begin{bmatrix} 0 \\ 1 \end{bmatrix} \quad (8b)$$

A discrete-time system having identical states with (8) at $t = kT_s$, with T_s the sampling time and $k \in N_0$, is:

$$\mathbf{x}_i^e(k+1) = \mathbf{E}_i^e(T_s)\mathbf{x}_i^e(k) + \mathbf{f}_i^e(T_s)(u_i^*(k) + \nu_i(k)) \quad (9a)$$

where k and $k+1$ abbreviate kT_s and $(k+1)T_s$, and

$$\mathbf{E}_i^e = e^{\mathbf{A}_i^e T_s} = \begin{bmatrix} 1 & T_s \\ 0 & 1 \end{bmatrix}, \ \mathbf{f}_i^e = \int_0^{T_s} e^{\mathbf{A}_i^e \xi} \mathbf{b}_i^e d\xi = \begin{bmatrix} T_s^2/2 \\ T_s \end{bmatrix} \quad (9b)$$

The DSMC design, presented in the next subsection, assumes availability of both elements of $\mathbf{x}_i^e$. If only joint positions are measured, and the measurements feature a time-delay of $\psi = pT_s$ ($p \in N_0$), then a Kalman observer technique [10,11] can be used to reconstruct the vector of states $\mathbf{x}_i^e$. To apply this technique, we define the continuous-time output equation:

$$\begin{aligned} y_i(t) &= q_i(t - \psi) + \eta_i(t) \\ &= q_{r,i}(t - \psi) + e_i(t - \psi) + \eta_i(t), \end{aligned} \quad (10)$$

where y_i is the observed output and η_i is the measurement noise. The standard assumption for ν_i is that it is an integral of the white process noise ζ_i [11]:

$$\dot{\nu}_i(t) = \zeta_i(t) \quad (11)$$

By virtue of (10) and (11), the discrete-time system (9) can be extended as follows:

$$\begin{aligned} &\mathbf{x}_i(k+1) = \mathbf{E}_i(T_s)\mathbf{x}_i(k) + \mathbf{f}_i(T_s)u_i^*(k) + \boldsymbol{\gamma}_i(T_s)\zeta_i(k); \\ &y_i(k) = q_{r,i}(k - p) + \mathbf{c}_i^T \mathbf{x}_i(k) + \eta_i(k), \end{aligned} \quad (12a)$$

where

$$\mathbf{x}_i(k) = [e_i(k-p), e_i(k-p+1), \ldots, e_i(k), \dot{e}_i(k), \nu_i(k)]^T.$$

$$\mathbf{E}_i(T_s) = \begin{bmatrix} \mathbf{E}_i^a & \mathbf{E}_i^b \\ \mathbf{E}_i^c & \mathbf{E}_i^d \end{bmatrix}, \ \mathbf{E}_i^a = \mathbf{0}_{p\times 1}, \ \mathbf{E}_i^b = [\mathbf{I}_p, \mathbf{0}_{p\times 2}],$$

$$\mathbf{E}_i^c = \mathbf{0}_{3\times p},$$

$$\mathbf{E}_i^d = \begin{bmatrix} 1 & T_s & T_s^2/2 \\ 0 & 1 & T_s \\ 0 & 0 & 1 \end{bmatrix}, \ \mathbf{f}_i = [\mathbf{0}_{1\times p}, T_s^2/2, T_s, 0]^T,$$

$$\boldsymbol{\gamma}_i = [\mathbf{0}_{1\times p}, T_s^3/6, T_s^2/2, T_s]^T, \ \mathbf{c}_i = [1, \mathbf{0}_{1\times(p+2)}]^T. \quad (12b)$$

Here, $\mathbf{I}_p \in \mathbb{R}^{p\times p}$ is the identity matrix, and $\mathbf{0}_{mxn} \in \mathbb{R}^{m\times n}$ contains zeros only. With the state-space representation (12), a Kalman observer can be designed to reconstruct the states $\mathbf{x}_i$ in the presence of time-delay and noise η_i, according to:

$$\begin{aligned} &\hat{\mathbf{x}}_i(k+1) = \mathbf{E}_i(T_s)\bar{\mathbf{x}}_i(k) + \mathbf{f}_i(T_s)u_i^*(k), \\ &\bar{\mathbf{x}}_i(k) = \hat{\mathbf{x}}_i(k) + \mathbf{k}_i[y_i(k) - \mathbf{c}_i^T \hat{\mathbf{x}}_i(k)]. \end{aligned} \quad (13)$$

where $\bar{\mathbf{x}}_i$ denotes the updated estimate of all states, and $\mathbf{k_i} \in \mathbb{R}^{p+3}$ is a vector of constant gains determined by the forms of $\mathbf{E}_i$ and γ_i, and the properties of ζ_i and η_i [10,11].

C. Design of a Discrete-time Sliding Mode Controller

The DSMC design [8] of the feedback control law u_i^* is based on the following representation of (9):

$$\delta\mathbf{x}_i^e(k) = \mathbf{A}_i^\delta \mathbf{x}_i^e(k) + \mathbf{b}_i^\delta(T_s)(u_i^*(k) + \nu_i(k)). \quad (14a)$$

where

$$\delta\mathbf{x}_i^e(k) = (\mathbf{x}_i^e(k+1) - \mathbf{x}_i^e(k))/T_s,$$

$$\mathbf{A}_i^\delta = (\mathbf{E}_i^e - \mathbf{I}_2)/T_s = \begin{bmatrix} 0 & 1 \\ 0 & 0 \end{bmatrix}, \ \mathbf{b}_i^\delta = \mathbf{f}_i^e/T_s = \begin{bmatrix} T_s/2 \\ 1 \end{bmatrix} \quad (14b)$$

The pair $(\mathbf{A}_i^\delta, \mathbf{b}_i^\delta)$ is controllable for any T_s. The feedback control law should be formulated in terms of $\bar{\mathbf{x}}_i^e(k) = [\bar{e}_i(k), \bar{\dot{e}}_i(k)]^T$, where $\bar{e}_i(k)$ and $\bar{\dot{e}}_i(k)$ are from (13).

The switching function is based on $\bar{\mathbf{x}}_i^e$

$$s_i(k) = \boldsymbol{\lambda}_i^T \bar{\mathbf{x}}_i^e(k), \ \boldsymbol{\lambda}_i = [\lambda_i^p \ \ \lambda_i^d]^T \quad (15)$$

where $s_i, \lambda_i^p, \lambda_i^d \in \mathbb{R}$ and $(\lambda_i^p, \lambda_i^d) \neq (0,0)$. The reaching law approach [2,3,6-8] is used for the controller design:

$$\delta s_i(k) = (s_i(k+1) - s_i(k))/T_s = \boldsymbol{\lambda}_i^T \delta \bar{\mathbf{x}}_i^e(k) = \\ = -\phi(s_i(k)), \tag{16}$$

where ϕ should be chosen such that the system state trajectories reach in finite time

1) the switching manifold $s_i = 0$ in the absence of disturbances and modeling errors; as $s_i = 0$ is reached, the states should remain on the manifold, establishing chattering-free control (contrary to the discrete-time quasi-sliding mode [6], no zigzagging about $s_i = 0$ should occur; the system motions must remain stable and stick to $s_i = 0$),
2) a close vicinity of $s_i = 0$ in the presence of disturbances and modeling errors; within the vicinity, chattering-free control should arise.

In the following, two spaces will be considered:

1) the *state space*, with $\bar{\mathbf{x}}_i^e$ $(i=1,..,n)$ as coordinates,
2) the *reaching space* [6], with s_i $(i=1,..,n)$ as coordinates.

The feedback control law is found as in [8]–if (14a,b) is substituted into (16), $\nu_i(k)$ is omitted since it is considered unknown, and (15) is taken into account, one determines:

$$u_i^*(k) = -\frac{\boldsymbol{\lambda}_i^T \mathbf{A}_i^\delta}{\boldsymbol{\lambda}_i^T \mathbf{b}_i^\delta(T_s)} \bar{\mathbf{x}}_i^e(k) - \frac{\phi(s_i(k))}{\boldsymbol{\lambda}_i^T \mathbf{b}_i^\delta(T_s)} \\ = -\frac{\lambda_i^p \dot{\bar{e}}_i(k) + \phi(s_i(k))}{0.5T_s\lambda_i^p + \lambda_i^d}. \tag{17}$$

An appropriate ϕ should ensure that (17) is stabilizing for the system (14) in the presence of ν_i. Next, sufficient conditions are formulated that an appropriate ϕ must fulfill.

Consider the system (14) with control (17). We use the following three assumptions.

(*i*) The collection of model uncertainties and disturbances is assumed bounded according to $|\nu_i(k)| \leq \mu_i$, $\forall k \in N_0$.

(*ii*) The vicinity of the switching manifold $s_i = 0$ is assumed to be given by $S_i^{ss} = \{\bar{\mathbf{x}}_i^e \in \mathbb{R}^2 : |\boldsymbol{\lambda}_i^T \bar{\mathbf{x}}_i^e(k)| < \varepsilon_i T_s\}$ in the state space, or $S_i^{rs} = \{s_i \in \mathbb{R} : |s_i(k)| < \varepsilon_i T_s\}$ in the reaching space.

(*iii*) The state reconstruction (13) is assumed to ensure: $\bar{\mathbf{x}}_i^e(k) \equiv \mathbf{x}_i^e(k)$.

The next theorem is obtained by adapting Theorems 1 and 2 from [8] for the considered robot control problem.

Theorem 1. In order that for any initial $\bar{\mathbf{x}}_i^e(0) \equiv \mathbf{x}_i^e(0)$ there exists a number $K = K(\bar{\mathbf{x}}_i^e(0))$, such that $\bar{\mathbf{x}}_i^e(k) \in S_i^{ss}$ for $k \geq K$, it is sufficient that the following conditions hold:

(*iv*) $\phi = s_i(k)/T_s$ for $s_i(k) \in S_i^{rs}$,

(*v*) $o_i T_s \mu_i / |s_i(k)| < T_s \phi(s_i(k))/s_i(k) < 1$, for $s_i(k) \notin S_i^{rs}$, $o_i > \boldsymbol{\lambda}_i^T \mathbf{b}_i^\delta(T_s)$,

(*vi*) $\varepsilon_i > \mu_i \left| \boldsymbol{\lambda}_i^T \mathbf{b}_i^\delta(T_s) \right|$.

If $\nu_i \equiv 0$, then to have $s_i(k) = 0$ for $k > K(\bar{\mathbf{x}}_i^e(0))$, it is sufficient if (*iv*) holds and $0 < T_s\phi/s_i < 1$ is satisfied for $s_i \notin S_i^{rs}$.

Proof. Similar to proofs of Theorems 1 and 2 from [8]. ■

Dead-beat property: if $\nu_i \equiv 0$, then (*iv*) is the necessary and sufficient condition for reaching $s_i = 0$ in one step, after $\bar{\mathbf{x}}_i^e$ enters S_i^{ss} [8].

One choice of ϕ, suggested in [8], is

$$\phi(s_i) = \begin{cases} s_i/T_s \text{ if } s_i \in S_i^{rs}; \\ \rho_i s_i + \sigma_i \operatorname{sgn}(s_i) \text{ if } s_i \notin S_i^{rs}, \end{cases} \\ 0 \leq \rho_i T_s < 1, \quad \sigma_i > o_i \mu_i \underset{(v)}{>} \boldsymbol{\lambda}_i^T \mathbf{b}_i^\delta(T_s) \mu_i \tag{18}$$

where

$$S_i^{rs} = \{s_i \in \mathbb{R} : |s_i(k)| < \sigma_i T_s/(1-\rho_i T_s)\} \tag{19a}$$

$$S_i^{ss} = \{\bar{\mathbf{x}}_i^e \in \mathbb{R}^2 : |\boldsymbol{\lambda}_i^T \bar{\mathbf{x}}_i^e(k)| < \sigma_i T_s/(1-\rho_i T_s)\} \tag{19b}$$

Within S_i^{rs}, u_i^* defined by (17) is a continuous function of the states (see (18) and (15)), providing the chattering-free DSMC.

D. Discrete-time Sliding Mode Controller Tuning

In this part we discuss tuning of the coefficients present in the feedback control law (17), with ϕ defined by (18). Since by virtue of (14b) and (15), $\boldsymbol{\lambda}_i^T \mathbf{b}_i^\delta(T_s) = 0.5T_s\lambda_i^p + \lambda_i^d$, then (18) implies $\sigma_i > (0.5T_s\lambda_i^p + \lambda_i^d)\mu_i$. According to (*i*), μ_i must overbound v_i, which is reconstructed with $\bar{\nu}_i$. The coefficient ρ_i is subject to $0 \leq \rho_i T_s < 1$, where higher ρ_i speeds up reaching S_i^{rs} [3,6].

The coefficients λ_i^p and λ_i^d of the switching function s_i, in (15), should be chosen such that the dynamics of the system (9) with control (17), is stable within S_i. So far we considered $\bar{\mathbf{x}}_i^e \equiv \mathbf{x}_i^e$ (see (*iii*)). We assume now:

$$e_i = \bar{e}_i + \Delta e_i, \ \dot{e}_i = \dot{\bar{e}}_i + \Delta \dot{e}_i \text{ with } |\Delta e_i| < \infty, \ |\Delta \dot{e}_i| < \infty \tag{20}$$

By virtue of (18), if $s_i \in S_i^{rs}$, then (17) defines a conventional PD (proportional, derivative) control action:

$$u_i^*(k) = -\kappa_i^p \bar{e}_i(k) - \kappa_i^d \dot{\bar{e}}_i(k) \tag{21a}$$

$$\kappa_i^p = \frac{\beta_i}{T_s(0.5T_s\beta_i + 1)}, \ \kappa_i^d = \frac{T_s\beta_i + 1}{T_s(0.5T_s\beta_i + 1)}, \ \beta_i = \frac{\lambda_i^p}{\lambda_i^d} \tag{21b}$$

The proportional and derivative gains κ_i^p and κ_i^d, respectively, are uniquely defined by β_i –the slope of the switching line $s_i = 0$ (see (15)). If we apply (21) to (9), and take (20) into account, we obtain:

$$\begin{bmatrix} e_i(k+1) \\ \dot{e}_i(k+1) \end{bmatrix} = \frac{1}{0.5T_s\beta_i + 1}\begin{bmatrix} 1 & 0.5T_s \\ -\beta_i & -0.5T_s\beta_i \end{bmatrix}\begin{bmatrix} e_i(k) \\ \dot{e}_i(k) \end{bmatrix} + \begin{bmatrix} 0.5T_s^2 \\ T_s \end{bmatrix} \cdot \cdot \left(\nu_i(k) + \frac{\beta_i \Delta e_i(k) + (T_s\beta_i + 1)\Delta\dot{e}_i(k)}{T_s(0.5T_s\beta_i + 1)} \right). \quad (22)$$

Since ν_i, Δe_i, and $\Delta\dot{e}_i$ are assumed bounded, the necessary and sufficient condition to have the magnitudes of the states of (22) monotonically decreasing is found as

$$-1 < (1 - 0.5T_s\beta_i)/(1 + 0.5T_s\beta_i) < 1 \Leftrightarrow \beta_i = \lambda_i^p / \lambda_i^d > 0 \quad (23)$$

assuming $T_s > 0$.

As already mentioned, the PD gains in (21b) are uniquely defined by β_i. This seems a main shortcoming of the considered DSMC algorithm when used in robot motion control. In Fig. 1, we plot κ_i^p and κ_i^d against β_i ($T_s = 1$ ms). In the same figure, we show $2\sqrt{\kappa_i^p}$, a common choice for the derivative gain for continuous-time second order systems (relative damping equal to one) [12]. Of course, the equivalence with continuous systems is sensible only for small sampling times, realistic in modern robotics. The middle plot was obtained by zooming the top of the figure for $0 \le \beta_i \le 1.5$. Apparently, $\kappa_i^p < \kappa_i^d$ for $\beta_i < 1$. From the bottom plot, one notices the rising tendency of $2\sqrt{\kappa_i^p}$. Up to $\beta_i = 414$, κ_i^d is higher than $2\sqrt{\kappa_i^p}$, implying relative damping above one. As κ_i^p is limited by the maximal feasible closed-loop bandwidth, realistic β_i cannot be high. For lower β_i, κ_i^d is much larger than $2\sqrt{\kappa_i^p}$, implying high relative damping. High damping, induced by the dead-beat property implied by (*iv*), may amplify noise considerably and excite parasitic dynamics (e.g. flexibility) at higher frequencies. These unwanted effects are inherent to control chattering arising with nonideal sliding mode control [1-3]. The considered DSMC algorithm was designed to establish chattering-free control, but, unfortunately, it fails in eliminating the unwanted effects. It appears that these effects can easily arise in practical implementations of the DSMC algorithm, and their negative influence on the control performance will be experimentally demonstrated in section IV.

III. Experimental Set-up

The robotic manipulator shown in Fig. 2, is an experimental facility for research in motion control [13-16]. Its *n*=3 revolute joints (RRR kinematics) are actuated by gearless brushless DC direct-drive motors. The actuators are Dynaserv DM-series servos with nominal torques of 60, 30, and 15 Nm, respectively. Each actuator has an integrated incremental optical encoder with a resolution of ~10^{-5} rad. The servos are driven by power amplifiers with built in current controllers. The joints have infinite range of motions, since the power and the sensor signals are transferred via sliprings. Both encoders and amplifiers are connected to a PC-based control system. This system consists of the MultiQ I/O board from Quanser Consulting, combined with a realtime controller for Matlab/Simulink (Wincon). This facilitates control designs in Simulink and real-time implementation. Typically, the controllers run with $T_s = 1$ ms sampling time.

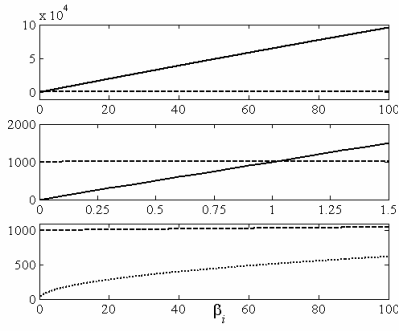

Fig. 1. Feedback gains: κ_i^p (solid), κ_i^d (dashed), and $2\sqrt{\kappa_i^p}$ (dotted).

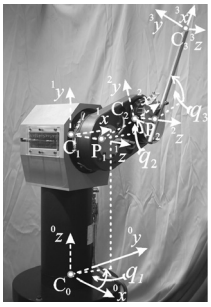

Fig. 2. The RRR robot.

TABLE I. Denavits-Hartenberg's Parameters of the RRR Robot

i	α_i [rad]	a_i [m]	q_i	d_i [m]
1	$\pi/2$	0	q_1	C_0C_1=0.560
2	0	P_1C_2=0.200	q_2	C_1P_1=0.169
3	0	P_2C_3=0.415	q_3	C_2P_2=0.090

Closed-form models of the robot kinematics and rigid-body dynamics are available in [14]. Their kinematic parameters, according to the well-known Denavits-Hartenberg's notation [12], are presented in Table 1. The inertial and friction parameters are estimated with sufficient accuracy in [13]. During motion control, the nonlinearity and couplings in the robot dynamics are reduced using (2), based on the rigid-body dynamic model. Information about the flexible dynamics are obtained by identification. For illustration, Fig. 3 presents the frequency response function (FRF) of the dynamics in joint 1, identified from N data points measured on the robot: the feedback control action $\{u_1(k)\}_{k=1,\ldots,N}$ from (2) was the excitation, and the reconstructed joint angular response $\{\bar{q}_1(k)\}_{k=1,\ldots,N}$ was the response. The response was computed as $\bar{q}_1(k) = q_{r,1}(k) + \bar{e}_1(k)$, where $q_{r,1}$ was the known reference motion, and $\bar{e}_1$ was reconstructed according to (13). Practical procedures to identify an FRF as shown in Fig. 3 are explained in [15,16]. Note that the given FRF represents the dynamics of joint 1, as it was obtained by averaging the dynamics identified for different robot postures [16]. Together with the identified FRF, Fig. 3 shows an FRF of a double integrator, which, by virtue of (3), represents the rigid-body dynamics in the joint. By inspection of the plots depicted in Fig. 3, it can be noticed that the rigid-body dynamics dominate up to approximately 20 Hz. Due to insuf-

ficient stiffness in mounting the robot base to the floor, a resonance around 28 Hz is present at the base. Flexible effects at higher frequencies are also apparent. The phase plot of the identified FRF deviates from the ideal -180°, due to a time-delay of $\psi = 2T_s$ between u_1 and the observed output y_1 from (10) [15]. The output is corrupted with quantization noise η_1 from the incremental encoder. Flexible effects and time delay appear also in the other two joints, which were also identified.

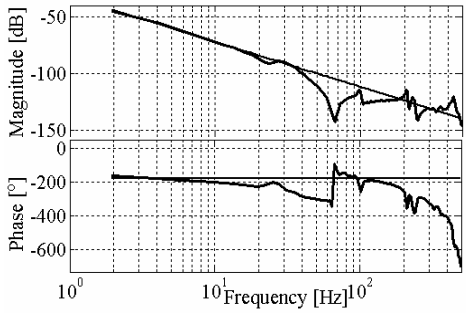

Fig. 3. FRFs of actual (thick) and ideal (thin) dynamics in joint 1.

IV. Feedback Control Design for the RRR Robot

Here, the DSMC feedback is illustrated for the first robot joint in more detail. Similar designs were performed for the other two joints. The experiments were done with all joints actuated at the same time. The considered motion task is presented in Fig. 4: each robot joint had to be displaced for 2π [rad] in 3 [s], with zero initial/terminal speed and acceleration. Initially, the reference motions were realized using (2) and (5), with PD feedback controllers:

$$\mathbf{u}^*(k) = -1000\mathbf{I}_3\bar{\mathbf{e}}(k) - 2\sqrt{1000}\mathbf{I}_3\dot{\bar{\mathbf{e}}}(k) \qquad (24)$$

The state reconstruction is of sufficient quality, since the differences between the measured outputs y_i, see (12), and the corresponding $\bar{q}_i(k-2) = q_{r,i}(k-2) + \bar{e}_i(k-2)$, $i = 1,2,3$, are all within [$-2\cdot10^{-4}$, $2\cdot10^{-4}$] [rad].

The reconstructed $\bar{v}_i$ ($i = 1,2,3$) were used to determine μ_i (i=1,2,3), according to condition (i) of Theorem 1. With μ_i available, we choose σ_i (i=1,2,3) according to the relation $\sigma_i > (0.5T_s\lambda_i^p + \lambda_i^d)\mu_i$. As seen in subsection II.D, the stability of the closed-loop system for $s_i \in S_i^{rs}$ depends only on the ratio $\beta_i = \lambda_i^p / \lambda_i^d$. Thus, we can reduce the number of tuning coefficients by choosing $\lambda_i^d = 1$ (i=1,2,3). By virtue of (23), any positive λ_i^p (i=1,2,3) ensures stability in closed-loop, which suggests that any closed-loop bandwidth should be achievable within S_i^{rs}. High bandwidths are preferable, as they enable realization of faster robot motions. Flexibilities limit the maximal feasible closed-loop bandwidth within S_1^{rs}, implying that arbitrary high $\lambda_1^p = \beta_1$ is not admissible with respect to the stability in closed-loop. By taking the FRF presented in Fig. 3 into account, it appears that only $\beta_1 \le 12$ ensures stability within S_1^{rs}. From Fig. 1 it is obvious that different β_i correspond to different tuning of the equivalent PD controller (21). For $\beta_1 \le 12$, the relative damping is unreasonably high, and may excite flexible dynamics and amplify quantization noise. An appropriate set of PD gains, away from the "stability" boundary β_1=12, can be found using loop-shaping, as explained in [15-17]. With this technique, a designer tunes the gains in (21) by varying λ_1^p, to make a compromise between the conflicting demands for high closed-loop bandwidths, acceptable control performance (e.g., tracking performance, rejection of disturbances, excitation of parasitic dynamics, etc.), and stability. The loop-shaping for the first joint achieved the compromise for the value of $\lambda_1^p = 5$. For the selected λ_1^p and $\lambda_1^d = 1$, σ_1 was found as $\sigma_1 > (2.5T_s + 1)\mu_1$. The remaining tuning coefficient in (18) is ρ_i, which is tentatively chosen equal to zero ($i = 1,2,3$). Experiments showed no need for higher ρ_i. Figs. 5 and 6 present the experimental results.

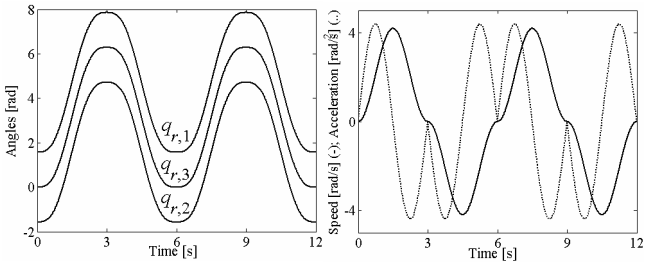

Fig. 4. The experimental motion task.

The left-hand side in Fig. 5 shows the online reconstructed errors achieved with DSMC controllers implemented in all three joints. The errors in joints 1 and 2 stay within the range [-10^{-3},10^{-3}] [rad], while in joint 3 the error peaks are almost three times higher. Closer inspection of the error plots reveals the presence of oscillatory components superimposed to the error patterns. The existence of these fine oscillations is confirmed by the errors' cumulative power spectra (CPS), shown on the right in Fig. 5. By inspection of the CPS plots, it can be seen that the dominant energy of the position error is in the lower frequency range, which is the range of the reference trajectory shown in Fig. 4. Outside this range, jumps in the slopes of the error CPSs are present around 20 Hz. These jumps are due to oscillations observed in the error signals. The oscillations correspond to severe peaking around 20 Hz in the sensitivity function [15-17], that can be computed using the identified FRF shown in Fig. 3 and the equivalent PD controller (21) with λ^p = 5. It appears that the oscillation arises in all three joints, because of elastic couplings not compensated using the rigid-body dynamic model implemented in (2).

The left-hand side of Fig. 6 shows the control torques computed using (2), with the feedback control action realized by (5) and (17). The chattering effect from the SMC theory is clearly eliminated, but the presence of oscillations,

related with the oscillation discussed in the previous paragraph, is obvious. The right-hand side of Fig. 6 presents $s_i(t)$ (i=1,2,3). The bounds of each plot of $s_i(t)$ match the bounds of S_i^{rs}. Apparently, each $s_i(t)$ remains within S_i^{rs}.

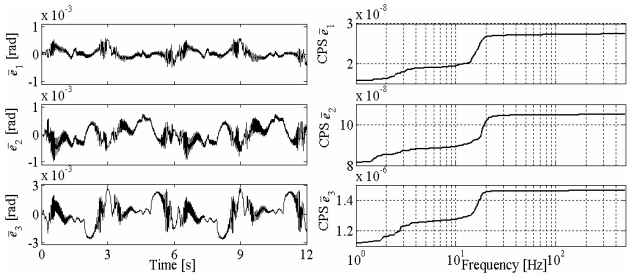

Fig. 5. Left: experimental position errors; right: errors' CPSs.

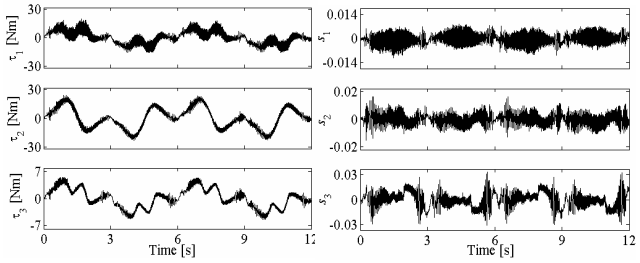

Fig. 6. Left: control torques; right: $s_i(t)$ (i=1,2,3).

It appears that the DSMC of the RRR robot does not give the performance achievable with H_∞ feedback control [15,16]. This could be expected, since H_∞ controllers are based on models with flexibilities included, while the DSMCs consider only the rigid-body dynamics that remains after feedback linearization. Furthermore, H_∞ controllers, as designed in [15,16], also include integral action, while the DSMCs considered in this paper do not. Additionally, as we could see in subsection II.D, there is a restriction in tuning the DSMC that impedes satisfactory loop-shaping within the vicinity of the switching manifold. This restriction can easily cause excitation of flexibilities in robotic systems. We intend to investigate the DSMC design for the dynamics that include flexibilities. Such design will certainly increase the order of the resulting controller and of the accompanied Kalman observer. The expected merit, though, would be robust feedback control with nice and predictable transient characteristics.

V. Conclusions and Outlook

In this paper, a fair treatment of a recent discrete-time sliding mode control (DSMC) algorithm is given, and its utility for robot motion control is analyzed. With a theoretical analysis, as well as by experimental results, it is shown that the theoretical merits of the algorithm, namely, finite time reaching of ideal chattering-free DSMC and stability robustness against disturbances and modeling uncertainty, are achieved at the price of unreasonably high feedback gains that may cause undesirable effects: noise amplification and excitation of parasitic dynamics. It appears that even with very careful tuning, the considered DSMC algorithm can cause undesirable effects in a robotic system, degrading the performance of motion control. Using a model that includes flexible dynamics, is the possible improvement to be investigated in the future.

Acknowledgment

The authors wish to thank to dr. Goran Golo for initiating the experimental work presented in the paper, and for useful discussions about the discrete-time sliding mode control approach.

References

[1] V.I. Utkin, Sliding Modes in Control Optimization, Springer-Verlag, Berlin, 1992.

[2] J.Y. Hung, W. Gao, and J.C. Hung, "Variable Structure Control: A Survey," IEEE Trans. on Indust. Elect., vol. 40, no. 1, pp. 2-22, 1993.

[3] W. Gao and J.C. Hung, "Variable Structure Control of Nonlinear Systems: A New Approach," IEEE Trans. on Indust. Elect., vol. 40, no. 1, pp. 45-55, 1993.

[4] J.J.E. Slotine and W. Li, Applied nonlinear control, Prentice-Hall, Upper Saddle River, NJ, 1991.

[5] Č. Milosavljević, "General Conditions for the Existence of a Quasi-sliding Mode on the Switching Hyperplane in Discrete Variable Structure Systems," Autom. Remote Control, vol. 46, pp. 307-314, 1985.

[6] W. Gao, Y. Wang, and A. Homaifa, "Discrete-time Variable Structure Control Systems," IEEE Trans. on Indust. Elect., vol. 42, no. 2, pp. 117-122, 1995.

[7] G. Golo and Č. Milosavljević, "Two-phase Triangular Wave Oscillator Based on Discrete-time Sliding Mode Control," Electronic Letters, vol. 33, no. 22, pp. 1838-1839, 1997.

[8] G. Golo and Č. Milosavljević, "Robust Discrete-time Chattering Free Sliding Mode Control," Syst. & Control Let., vol. 41, no. 1, pp. 19-28, 2000.

[9] M. Vukobratović and V. Potkonjak, Dynamics of Manipulation Robots: Theory and Application, Springer-Verlag, Berlin, 1982.

[10] A. Gelb, Applied Optimal Estimation, The M.I.T. Press, London, 1996.

[11] P.R. Bélanger, P. Dobrovolny, A. Helmy, and X. Zhang, "Estimation of Angular Velocity and Acceleration from Shaft-Encoder Measurements," Int. J. Rob. Res., vol. 17, no. 11, pp. 1225-1233, 1998.

[12] L. Sciavicco and B. Siciliano, Modeling and Control of Robot Manipulators, McGraw-Hill, London, 1996.

[13] D. Kostić, R. Hensen, B. de Jager, and M. Steinbuch, "Modeling and Identification of an RRR-robot," Proc. IEEE Conf. Dec. Control, pp. 1144-1149, Orlando, FL, 2001.

[14] D. Kostić, R. Hensen, B. de Jager, and M. Steinbuch, "Closed-form Kinematic and Dynamic Models of an Industrial-like RRR Robot," Proc. IEEE Conf. Rob. Autom. pp. 1309-1314, Washington D.C., 2002.

[15] D. Kostić, B. de Jager, and M. Steinbuch, "Experimentally Supported Control Design for a Direct Drive Robot," Proc. IEEE Int. Conf. Control Appl., pp. 186-191, Glasgow, Scotland, 2002.

[16] D. Kostić, B. de Jager, M. Steinbuch, "Control Design for Robust Performance of a Direct-drive Robot," Proc. IEEE Int. Conf. Control Appl., pp. 1448-1453, Istanbul, Turkey, 2003.

[17] M. Steinbuch and M.L. Norg, "Advanced Motion Control," Europ. J. Control, vol. 4, no. 4, pp. 278-293, 1998.